

Acoustic radiation force and torque on a lossless eccentric layered fluid cylinder

F G Mitri

Citation: Chin. Phys. B .2020, 29 (**11**): 114302. **doi:** 10.1088/1674-1056/aba27a
Journal homepage: http://cpb.iphy.ac.cn; http://iopscience.iop.org/cpb

What follows is a list of articles you may be interested in

Pulling force of acoustic-vortex beams on centered elastic spheres based on the annular transducer model

Yuzhi Li(李禹志), Qingdong Wang(王青东), Gepu Guo(郭各朴), Hongyan Chu(褚红燕), Qingyu Ma(马青玉), Juan Tu(屠娟), Dong Zhang(章东)
Chin. Phys. B . 2020, 29(5): 054302 . **doi:** 10.1088/1674-1056/ab8210

Axial acoustic radiation force on a fluid sphere between two impedance boundaries for Gaussian beam

Yuchen Zang(臧雨宸), Yupei Qiao(乔玉配), Jiehui Liu(刘杰惠), Xiaozhou Liu(刘晓宙)
Chin. Phys. B . 2019, 28(3): 034301 . **doi:** 10.1088/1674-1056/28/3/034301

Acoustic radiation force on a multilayered sphere in a Gaussian standing field

Haibin Wang(汪海宾), Xiaozhou Liu(刘晓宙), Sha Gao(高莎), Jun Cui(崔骏), Jiehui Liu(刘杰惠), Aijun He(何爱军), Gutian Zhang(张古田)
Chin. Phys. B . 2018, 27(3): 034302 . **doi:** 10.1088/1674-1056/27/3/034302

Random phase screen influence of the inhomogeneous tissue layer on the generation of acoustic vortices

Zhiyao Ma(马致遥), Jun Ma(马骏), Dong Zhang(章东), Juan Tu(屠娟)
Chin. Phys. B . 2018, 27(3): 034301 . **doi:** 10.1088/1674-1056/27/3/034301

Acoustic radiation force induced by two Airy-Gaussian beams on a cylindrical particle

Sha Gao(高莎), Yiwei Mao(毛一葳), Jiehui Liu(刘杰惠), Xiaozhou Liu(刘晓宙)
Chin. Phys. B . 2018, 27(1): 014302 . **doi:** 10.1088/1674-1056/27/1/014302

Acoustic radiation force and torque on a lossless eccentric layered fluid cylinder

F G Mitri†

Santa Fe, NM 87508, *USA*

(Received 26 May 2020; revised manuscript received 24 June 2020; accepted manuscript online 2020)

Exact analytical equations and computations for the longitudinal and transverse acoustic radiation force and axial torque components for a lossless eccentric liquid cylinder submerged in a nonviscous fluid and insonified by plane waves progressive waves (of arbitrary incidence in the polar plane) are established and computed numerically. The modal matching method and the translational addition theorem in cylindrical coordinates are used to derive exact mathematical expressions applicable to any inner and outer cylinder sizes without any approximations, and taking into account the interaction effects between the waves propagating in the layer and those scattered from the cylindrical core. The results show that longitudinal and transverse radiation force components arise, in addition to the emergence of an axial radiation torque component acting on the non-absorptive compound cylinder due to geometrical asymmetry as the eccentricity increases. The computations demonstrate that the axial torque component, which arises due to a geometrical asymmetry, can be positive (causing counter-clockwise rotation in the polar plane), negative (clockwise rotation) or neutral (rotation cancellation) depending on the size parameter of the cylinder and the amount of eccentricity. Furthermore, verification and validation of the results have been accomplished from the standpoint of energy conservation law applied to scattering, and based on the reciprocity theorem.

Keywords: acoustic radiation force, acoustic radiation torque, non-viscous liquid eccentric cylinder

PACS: 43.25.Qp, 43.25.+y, 43.20.+g, 43.35.+d **DOI:** 10.1088/1674-1056/aba27a

Elongated particles in the form of cylindrical entities with circular geometrical cross-sections submerged in a non-viscous host fluid are commonly investigated as canonical objects in the study of the linear acoustic momentum transfer, and the generation of a time-averaged (steady-state) radiation force. Many analyses considering plane progressive and standing waves impinging on a rigid (sound impenetrable) or movable cylinder[1] perpendicularly to its axis have been undertaken[2,3] and later extended to take into account the material elasticity[4–8] and sound absorption inside the core cylinder[8,9] or cylindrical shells.[10] Formalisms accounting for the viscosity of the host fluid medium have been also developed.[11,12] Lately, further extensions to take into account the shape of the incident insonifying wave-field (differing from plane waves) have been considered,[13,14] and showed interesting properties for non-paraxial focused Gaussian,[15] Hermite–Gaussian,[16] and Airy[17,18] acoustical sheet tweezers from the standpoint of negative pulling force generation acting in opposite direction of wave motion, and linear, parabolic and reverse particle transport.

To date, the published literature on radiation force has been mainly focused on cylinders and cylindrical shells with a concentric core (*i.e.*, zero eccentricity).[5,6,10] When the eccentricity increases (*i.e.*, $d \neq 0$, see Fig. 1), previous works showed that the linear acoustic scattering[19–21] is significantly altered; bifurcation and resonance shifting occur, which amount to the degree of eccentricity.[22,23] How eccentricity affects the time-averaged radiation force remains to be further explored, which constitutes the main objective of this study. Interestingly, in addition to the radiation force effect, this work shows that a novel effect related to the time-averaged radiation torque (causing particle rotation) about its center of mass arises as well, which is not associated with sound absorption[15] as the eccentric fluid layered cylinder considered here is non-viscous. Rather, the acoustic radiation torque emerges as a consequence of geometrical asymmetry with respect to the axis of the compound cylindrical particle (*i.e.*, eccentricity $d \neq 0$, Fig. 1) as it will be demonstrated in the following.

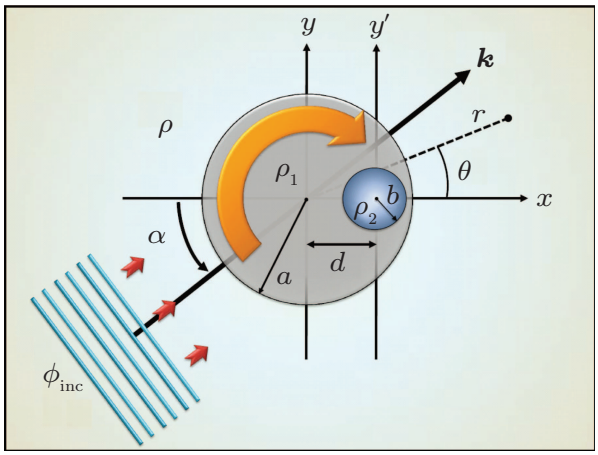


Fig. 1. Graphical representation for the interaction of acoustical plane progressive waves (with arbitrary incidence in the polar plane) with an eccentric lossless fluid layered cylinder of arbitrary size. The rotating arrow denotes the axial radiation torque component generated with respect to center of mass of the compound cylinder of radius a, coating the one with radius b.

†Corresponding author. E-mail: F.G.Mitri@ieee.org

© 2020 Chinese Physical Society and IOP Publishing Ltd

Consider incident acoustical plane progressive waves propagating in an unbounded nonviscous fluid at an arbitrary angle α (in the polar plane) with respect to the center of a compound eccentric layered fluid cylinder, as shown in Fig. 1. For the purpose of the present study, the effects of viscosity of the host fluid medium and eccentric fluid cylinder, acoustic streaming, and surface tension are not considered, as they are deemed negligible for the conditions and examples chosen to illustrate the analysis. Using the partial-wave series expansion method in cylindrical coordinates,[24] the incident field is expressed by its incident velocity potential as

$$\varphi_{\rm inc}(r,\theta,t)=\varphi_0\,{\rm e}^{-{\rm i}\omega t}\sum_{n=-\infty}^{+\infty}{\rm i}^n\,{\rm e}^{-{\rm i}n\alpha}\,{\rm J}_n(kr)\,{\rm e}^{{\rm i}n\theta}, \tag{1}$$

where φ_0 is the amplitude, k $(=\omega/c)$ is the wavenumber in the medium of wave propagation, ω is the angular frequency, c is the speed of sound for the compressional wave, and ${\rm J}_n(\cdot)$ is the cylindrical Bessel function of the first kind.

In a lossless host fluid medium, surrounding the compound nonviscous fluid cylinder, the scattered velocity potential is expressed as

$$\varphi_{\rm sca}(r,\theta,t)=\varphi_0\,{\rm e}^{-{\rm i}\omega t}\sum_{n=-\infty}^{+\infty}C_n\,{\rm H}_n^{(1)}(kr)\,{\rm e}^{{\rm i}n\theta}, \tag{2}$$

where C_n are the modal coefficients, yet to be evaluated by applying adequate interfacial conditions,[19] and ${\rm H}_n^{(1)}(\cdot)$ is the cylindrical Hankel function of the first kind of order n.

The internal scalar fields corresponding to the compressional waves that exist in the layer (medium 1) and core (medium 2) lossless cylinders are also determined using exact partial-wave series, respectively, as

$$\begin{aligned}\varphi_{\rm int,1}=\ &\varphi_0\,{\rm e}^{-{\rm i}\omega t}\sum_{n=-\infty}^{+\infty}\Big[C_{n,1}^{\rm int}\,{\rm J}_n(k_1r)\,{\rm e}^{{\rm i}n\theta}\\&+D_{n,1}^{\rm int}\,{\rm H}_n^{(1)}\left(k_1r'\right){\rm e}^{{\rm i}n\theta'}\Big],\end{aligned} \tag{3}$$

$$\varphi_{\rm int,2}=\ \varphi_0\,{\rm e}^{-{\rm i}\omega t}\sum_{n=-\infty}^{+\infty}C_{n,2}^{\rm int}\,{\rm J}_n\left(k_2r'\right){\rm e}^{{\rm i}n\theta'}, \tag{4}$$

where $C_{n,1}^{\rm int}$, $D_{n,1}^{\rm int}$, and $C_{n,2}^{\rm int}$ are complex modal weighting coefficients for the waves in the fluid layer (medium 1) and core (medium 2), respectively. The parameters $k_{\{1,2\}}=\omega/c_{\{1,2\}}$ are the wavenumbers in the fluid media 1 and 2 with sound speeds $c_{\{1,2\}}$, respectively. To determine the modal coefficients, boundary conditions satisfying the continuity of the pressure and radial component of the particle velocity at each interface at $r=a$ [Eqs. (5) and (6) with $r>d$] and $r'=b$ [Eqs. (7) and (8)] must be satisfied.[19] Therefore, equations (1)–(4) must be expressed in both systems (r,θ) and (r',θ'). The transformation between the two systems of coordinates is performed adequately via the translational addition theorem for cylindrical wave functions.[25] The boundary conditions lead to a system of four equations with four unknowns (*i.e.*, C_n, $C_{n,1}^{\rm int}$, $D_{n,1}^{\rm int}$, and $C_{n,2}^{\rm int}$) that are determined by matrix inversion as in Refs. [26,27], obtained as

$${\rm i}^{\ell}{\rm J}_{\ell}(ka)\,{\rm e}^{-{\rm i}\ell\alpha}+C_{\ell}{\rm H}_{\ell}^{(1)}(ka)=C_{\ell,1}^{\rm int}{\rm J}_{\ell}(k_1a)+{\rm H}_{\ell}^{(1)}(k_1a)\sum_{n=-\infty}^{\infty}D_{n,1}^{\rm int}{\rm J}_{\ell-n}(k_1d), \tag{5}$$

$$\left(\frac{\rho_1c_1}{\rho c}\right)\left[{\rm i}^{\ell}{\rm J}_{\ell}'(ka)\,{\rm e}^{-{\rm i}\ell\alpha}+C_{\ell}{\rm H}_{\ell}^{(1)'}(ka)\right]=C_{\ell,1}^{\rm int}{\rm J}_{\ell}'(k_1a)+{\rm H}_{\ell}^{(1)'}(k_1a)\sum_{n=-\infty}^{\infty}D_{n,1}^{\rm int}{\rm J}_{\ell-n}(k_1d), \tag{6}$$

$$D_{\ell,1}^{\rm int}{\rm H}_{\ell}^{(1)}(k_1b)+{\rm J}_{\ell}(k_1b)\sum_{n=-\infty}^{\infty}C_{n,1}^{\rm int}{\rm J}_{n-\ell}(k_1d)=C_{\ell,2}^{\rm int}{\rm J}_{\ell}(k_2b), \tag{7}$$

$$D_{\ell,1}^{\rm int}{\rm H}_{\ell}^{(1)'}(k_1b)+{\rm J}_{\ell}'(k_1b)\sum_{n=-\infty}^{\infty}C_{n,1}^{\rm int}{\rm J}_{n-\ell}(k_1d)=\left(\frac{\rho_1c_1}{\rho_2c_2}\right)C_{\ell,2}^{\rm int}{\rm J}_{\ell}'(k_2b). \tag{8}$$

Based on the boundary conditions satisfying the continuity of the pressure and radial component of the particle velocity at each interface, the coefficients C_n used to compute the relevant physical observables, are shown to be coupled to $C_{n,1}^{\rm int}$ and $D_{n,1}^{\rm int}$ via Eqs. (5) and (6) [in addition to the coupling to the incident field], which in turn, are related to $C_{n,2}^{\rm int}$ as shown by Eqs. (7) and (8). Also, $D_{n,1}^{\rm int}$ is coupled to $C_{n,1}^{\rm int}$ as

$$D_{q,1}^{\rm int}=M_q\sum_{n=-\infty}^{+\infty}C_{n,1}^{\rm int}J_{n-q}(k_1d),$$

where

$$M_q=\left[\frac{{\rm J}_q(k_1b)\,{\rm J}_q'(k_2b)-(\rho_2c_2/\rho_1c_1)\,{\rm J}_q(k_2b)\,{\rm J}_q'(k_1b)}{(\rho_2c_2/\rho_1c_1)\,{\rm J}_q(k_2b)\,{\rm H}_q^{(1)'}(k_1b)-{\rm H}_q^{(1)}(k_1b)\,{\rm J}_q'(k_2b)}\right].$$

This coupling between the coefficients describes physically the interactions that occur between the waves propagating in each medium.

The analysis is now continued to derive analytically the exact mathematical expressions for the components of the acoustic radiation force and torque. The method is based on the far-field scattering approach since the compound cylinder is submerged in a non-viscous fluid medium. In this limit, the cylindrical Bessel and Hankel functions of the first kind are expressed, respectively, by the following functions:

$${\rm J}_n(\chi)\underset{\chi\to\infty}{\approx}\sqrt{\frac{2}{\pi\chi}}\cos\left(\chi-\frac{n\pi}{2}-\frac{\pi}{4}\right),$$

$${\rm H}_n^{(1)}(\chi)\underset{\chi\to\infty}{\approx}\sqrt{\frac{2}{\pi\chi}}\exp\left[{\rm i}\left(\chi-\frac{n\pi}{2}-\frac{\pi}{4}\right)\right],$$

and the radiation force and torque expressions are derived based on the integration of the acoustic radiation stress tensor and its moment over a surface at a large radius enclosing the layered compound eccentric cylinder.

The expression for the force vector derived previously[7] can be applied such that,

$$\langle \boldsymbol{F} \rangle \underset{kr\to\infty}{=} \frac{1}{2}\rho k^2 \int_0^{2\pi} \mathrm{Re}\left\{\Phi_{\mathrm{is}}(r,\theta,t)\right\} \mathrm{d}\boldsymbol{S}, \tag{9}$$

where $\mathrm{Re}\{\cdot\}$ denotes the real part of a complex number,

$$\Phi_{\mathrm{is}}(r,\theta,t) \underset{kr\to\infty}{=} \varphi^*_{\mathrm{sca}}\left[(\mathrm{i}/k)\left(\partial\varphi_{\mathrm{inc}}/\partial r\right) - \varphi_{\mathrm{inc}} - \varphi_{\mathrm{sca}}\right],$$

and $\mathrm{d}\boldsymbol{S} = \mathrm{d}S\,\boldsymbol{e}_r$, where $\mathrm{d}S = Lr\,\mathrm{d}\theta$ is the scalar differential element of a cylindrical surface S with a length L taken at a large radius enclosing the cylinder. $\boldsymbol{e}_r = \cos\theta\,\boldsymbol{e}_x + \sin\theta\,\boldsymbol{e}_y$, where $\boldsymbol{e}_x$ and $\boldsymbol{e}_y$ are the unit vectors in the Cartesian coordinates system, the symbol $\langle\cdot\rangle$ denotes time-averaging, and the superscript * denotes a complex conjugate. The longitudinal (*i.e.* along the x direction) and a transverse (*i.e.* along the y direction) components are expressed as

$$\left\{\begin{array}{c} F_x \\ F_y \end{array}\right\} = \langle \boldsymbol{F} \rangle \cdot \left\{\begin{array}{c} \boldsymbol{e}_x \\ \boldsymbol{e}_y \end{array}\right\} = \left\{\begin{array}{c} Y_x \\ Y_y \end{array}\right\} S_{\mathrm{c}} E_0, \tag{10}$$

where $S_{\mathrm{c}} = 2aL$ is the surface cross-section of the cylinder, $E_0 = (1/2)\rho k^2 |\varphi_0|^2$ is a characteristic energy density. The functions Y_x and Y_y are the longitudinal and transverse dimensionless efficiencies. The algebraic manipulation of Eq. (9) using the property of the angular integral,

$$\int_0^{2\pi} \mathrm{e}^{\mathrm{i}(n'-n)\theta} \left\{\begin{array}{c} \cos\theta \\ \sin\theta \end{array}\right\} \mathrm{d}\theta = \pi \left\{\begin{array}{c} (\delta_{n,n+1} + \delta_{n,n-1}) \\ \mathrm{i}\,(\delta_{n,n+1} - \delta_{n,n-1}) \end{array}\right\}, \tag{11}$$

leads to the exact analytical expressions for the longitudinal and transverse dimensionless components as

$$Y_x = \frac{1}{ka}\mathrm{Im}\left\{\sum_{n=-\infty}^{+\infty}\left(\mathrm{i}^n \mathrm{e}^{-\mathrm{i}n\alpha} + C_n\right)\left(C^*_{n+1} - C^*_{n-1}\right)\right\}, \tag{12}$$

$$Y_y = -\frac{1}{ka}\mathrm{Re}\left\{\sum_{n=-\infty}^{+\infty}\left(\mathrm{i}^n \mathrm{e}^{-\mathrm{i}n\alpha} + C_n\right)\left(C^*_{n+1} + C^*_{n-1}\right)\right\}, \tag{13}$$

where the symbol $\mathrm{Im}\{\cdot\}$ represents the imaginary part of a complex number.

As for the acoustic radiation torque, it is calculated as[28]

$$\langle \boldsymbol{N} \rangle \underset{kr\to\infty}{=} -\rho \iint_S \langle \boldsymbol{v} \otimes (\boldsymbol{r} \times \boldsymbol{v}) \rangle \cdot \mathrm{d}\boldsymbol{S}, \tag{14}$$

where the symbol $\otimes$ denotes a tensor product. $\boldsymbol{r}$ is the vector position, and $\boldsymbol{v} = \mathrm{Re}\nabla\{\varphi_{\mathrm{tot}}\} = \mathrm{Re}\{\nabla(\varphi_{\mathrm{inc}} + \varphi_{\mathrm{sca}})\}$. Due to geometry consideration, the only non-vanishing component of the time-averaged radiation torque vector [*i.e.*, in the direction perpendicular to the polar plane (r,θ)] can be rewritten as

$$N_z = \langle \boldsymbol{N} \rangle \cdot \boldsymbol{e}_z$$

$$= \frac{\rho}{2}\mathrm{Im}\left\{\int_0^{2\pi} \left(\partial\varphi^*_{\mathrm{tot}}/\partial r\right)\hat{L}_z\varphi_{\mathrm{tot}}\,\mathrm{d}S\right\}, \tag{15}$$

where φ_{tot} is given by the sum of Eqs. (1) and (2), $\boldsymbol{e}_z$ is the unit vector along the z direction, and $\hat{L}_z\left(=-\mathrm{i}\partial/\partial\theta\right)$ is the z component of the angular momentum operator in polar coordinates.

Manipulating the integral in Eq. (15) algebraically leads to the expression of the axial component of the radiation torque vector as

$$N_z = \tau_z V E_0, \tag{16}$$

where $V\,(=\pi a^2 L)$ is the volume, and τ_z is the non-dimensional axial radiation torque function, given by

$$\tau_z = -\frac{4}{\pi(ka)^2}\mathrm{Re}\left\{\sum_{n=-\infty}^{+\infty} n\left(\mathrm{i}^n \mathrm{e}^{-\mathrm{i}n\alpha} + C_n\right)C^*_n\right\}. \tag{17}$$

Equations (12), (13), and (17) written in mathematical partial-wave series constitute the main results of this analysis. They depend on the modal coefficients of the compound eccentric cylinder coupled to those of the incident plane progressive wave field. For adequate computational purposes, those infinite series are truncated at a maximum integer $N_{\max} = \mathrm{round}\,[ka + 4.05(ka)^{1/3} + 10]$ (largely exceeding ka) to warrant convergence.[29]

Those equations have been implemented by developing a MATLAB code. Programing and computations are performed using Eqs. (12), (13), and (17) for a non-viscous liquid-filled eccentric cylinder submerged in water ($\rho = 1000$ kg/m^3, $c = 1500$ m/s), and made of a high-density liquid, such as mercury ($\rho_1 = 13600$ kg/m^3, $c_1 = 1407$ m/s), with its core material made of water ($\rho_2 = \rho$, $c_2 = c$). The dimensionless size parameters kb and kd are fixed for each computation, and have taken particular discrete values to illustrate the analysis. The plots for Eqs. (12), (13), and (17) were varied in the ranges determined by $(kb+kd) < ka \leq 5 + (kb+kd)$, and $0 \leq \alpha \leq 180°$. To ensure the physicality of the results, the condition $a > (b+d)$ has been enforced throughout all the computations.

Panels (a) and (b) of Fig. 2 display the two-dimensional (2D) plots *versus* (ka, α) for the longitudinal and transverse radiation force efficiencies, respectively. The solid (black) line indicates the neutrality of the longitudinal radiation force efficiency (*i.e.*, $Y_x = 0$ for $\alpha = 90°$), as it should be expected. The inner fluid cylinder is located at the center of the large cylinder such that $kd = 0$, and $kb = 0.1$, corresponding to a Rayleigh (small) core. This configuration corresponds to a concentric (*i.e.*, $kd = 0$) cylindrical shell, and the asymmetry in panel (a) and symmetry in panel (b) *versus* $\alpha = 90°$ clearly demonstrates the lack of eccentricity. Panel (c) displays the plot for Eq. (17), which corresponds to the axial radiation torque efficiency τ_z that vanishes as required by the concentric symmetry. In addition, the plot for the extinction (or scattering) energy efficiency[30] for the lossless compound eccentric fluid

cylinder is displayed in panel (d), which has been calculated using the expression[30]

$$Q_{\rm ext} = -\frac{2}{ka}{\rm Re}\left\{\sum_{n=-\infty}^{+\infty} {\rm i}^n {\rm e}^{-{\rm i}n\alpha} C_n^*\right\} = Q_{\rm sca} = \frac{2}{ka}\sum_{n=-\infty}^{+\infty}|C_n|^2. \tag{18}$$

The symmetry in this plot versus the incidence angle value $\alpha = 90^\circ$ clearly verifies the accuracy of the results based on energy conservation and the reciprocity theorem.[31]

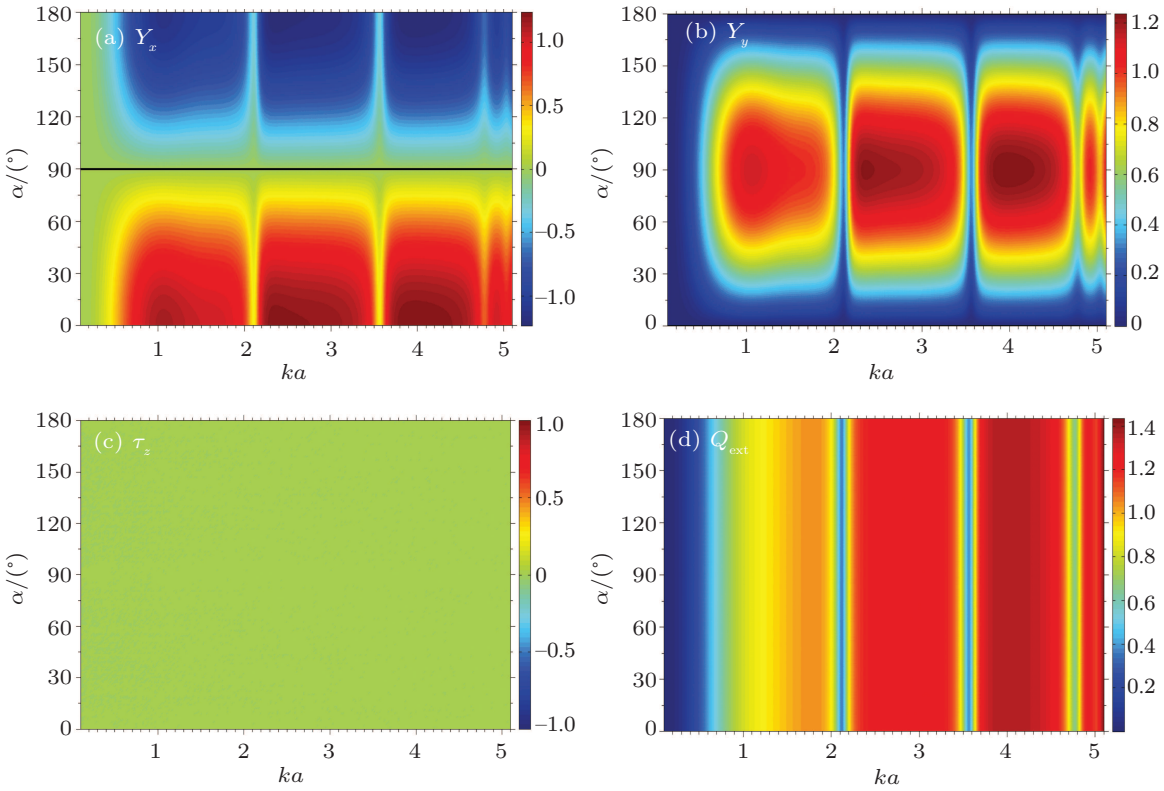


Fig. 2. Panels (a)–(d) display the two-dimensional plots *versus* (ka, α) of the dimensionless efficiencies Y_x, Y_y, τ_z, and $Q_{\rm ext}$, respectively, for $kd = 0$, $kb = 0.1$.

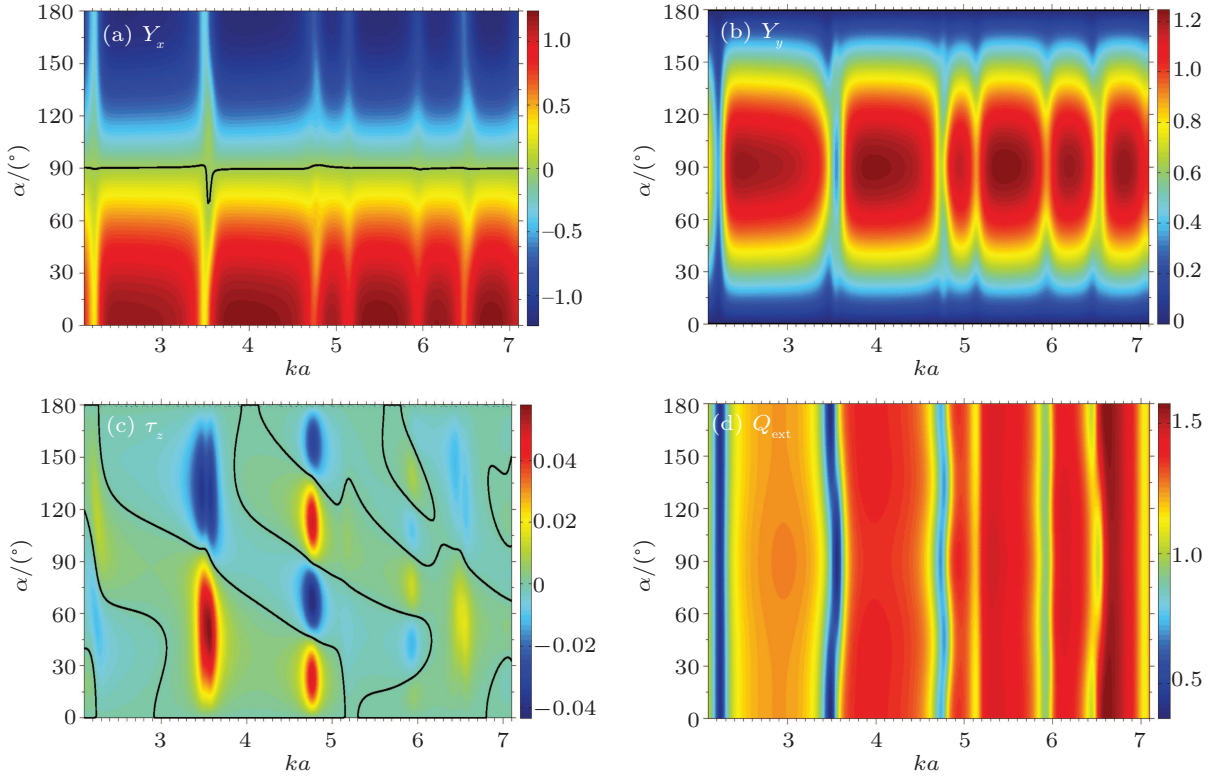


Fig. 3. Panels (a)–(d) display the two-dimensional plots *versus* (ka, α) of the dimensionless efficiencies Y_x, Y_y, τ_z, and $Q_{\rm ext}$, respectively, for $kd = 2$, $kb = 0.1$.

The effect of breaking the symmetry by increasing the eccentricity of the cylinder is investigated in Fig. 3, such that $kd = 2$, and $kb = 0.1$. Clearly, increasing the eccentricity breaks the symmetry and induces changes in the radiation force, torque and extinction/scattering efficiencies. The plot in panel (a) shows that an interesting effect arises; in the bandwidth $3.45 \leq ka \leq 3.55$ for incidence angle values $\alpha >\sim 68°$, Y_x is negative indicating that a negative longitudinal radiation force arises on the compound cylinder. This means that an attractive (pulling) force acting along the negative x direction (*i.e.*, in opposite direction of acoustical wave motion toward the acoustical source) arises. Total neutrality of Y_x is also achieved along the solid (black) line for $\alpha \approx 90°$. Panel (b) shows that the transverse radiation force efficiency Y_y is always positive and quasi-symmetric with respect to the incidence angle line $\alpha = 90°$ for the inner Rayleigh cylinder with $kb = 0.1$. The plot in panel (c) demonstrates the emergence of an axial radiation torque efficiency τ_z on the eccentric cylinder, in contrast to panel (c) of Fig. 2 for the concentric cylinder. Clearly, the eccentricity/asymmetry (*i.e.*, $kd \neq 0$) leads to the generation of an axial radiation torque component, which can be positive, negative, or zero along the solid (black) contour lines that surround the regions of positive and negative values. The positive to negative sign changes in the plot of τ_z indicate that depending on the values of (ka, α), counter-clockwise rotation in the polar plane, or clockwise rotation about the center of mass of the cylinder of radius a (Fig. 1) can occur. Neutrality (*i.e.*, $\tau_z = 0$) along the solid (black) lines indicates lack of rotation. Furthermore, the plot in panel (d) of Fig. 3 shows that Q_{ext} is always > 0, in agreement with the law of energy conservation.

The effect of increasing the inner cylinder radius is examined by choosing $kb = 5$, while keeping kd $(= 2)$ constant. The related results are displayed in panels (a)–(d) of Fig. 4. As shown in panel (a), increasing the size of the inner cylinder further leads to asymmetric longitudinal and transverse radiation force efficiencies; depending on the values of ka, Y_x, and Y_y varaying alternatively between positive or negative values while crossing zero as α varies. The plot in panel (c) shows a more complex form than the one observed in panel (c) of Fig. 3, where the solid (black) contour lines delimit well-defined "islands" over which a negative radiation torque efficiency arises; $\tau_z < 0$. Unlike the case of viscoelasticity,[15,32] the emergence of the axial radiation torque component as shown in panel (c) is solely related to the symmetry breaking versus the center of the non-viscous fluid eccentric cylinder of radius a as $kd \neq 0$ considered here. Comparisons of the plots in panel (c) of Figs. 3 and 4 show that τ_z is larger (in absolute sense) as kd increases. Moreover, panel (d) shows that symmetry *versus* the incidence angle value $\alpha = 90°$ is preserved and Q_{ext} is always > 0, which verifies the law of energy conservation applied to scattering.

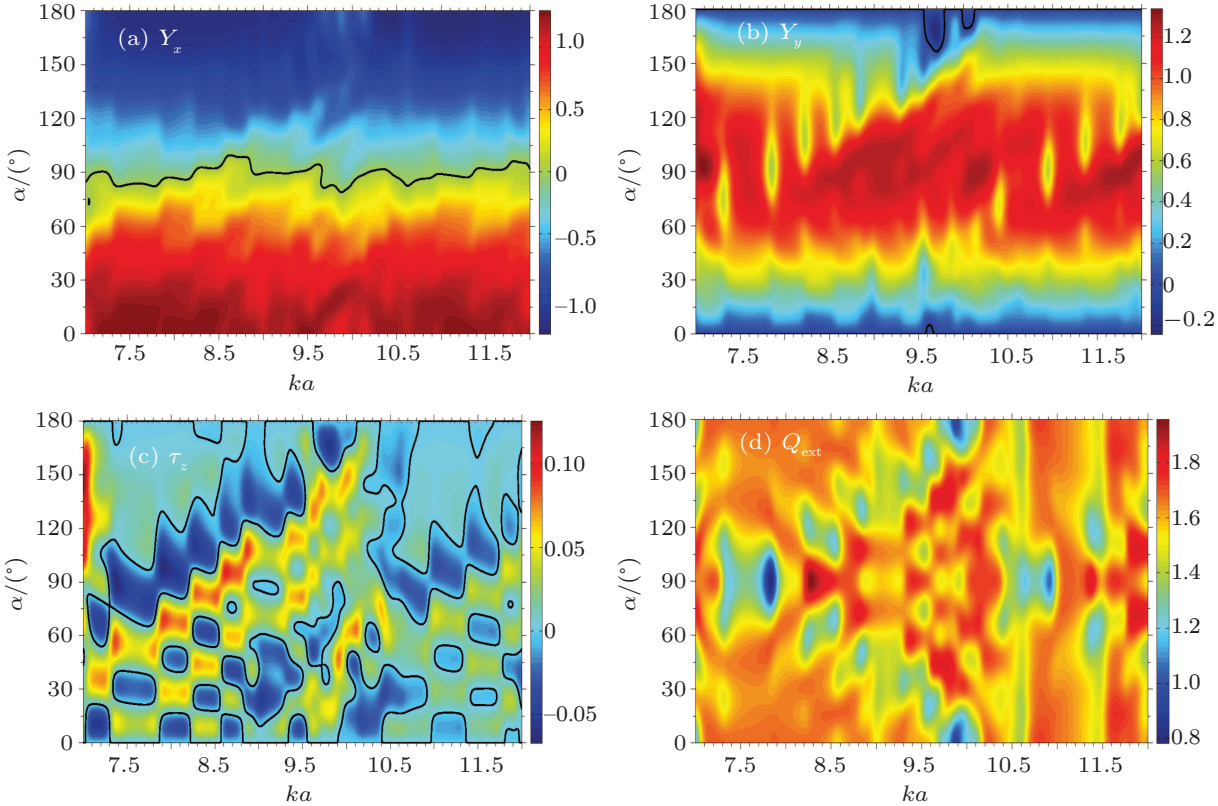


Fig. 4. Panels (a)–(d) display the two-dimensional plots *versus* (ka, α) of the dimensionless efficiencies Y_x, Y_y, τ_z, and Q_{ext}, respectively, for $kd = 2$, $kb = 5$.

In summary, this analysis provided exact expressions for the acoustic radiation force and torque components for an eccentric layered cylinder composed of a non-viscous inner core, layered by another non-viscous fluid shell material. Depending on the eccentricity of the cylinder, negative, positive or neutral radiation force and torque components arise depending on the size parameters of the layer *ka* and inner cylinder *kb* as well as the eccentricity *kd* and angle of incidence in the polar plane of the progressive waves. The results show that the axial radiation torque efficiency emerges, not as a result of absorption (as discussed previously in Refs [15,32]); it is rather connected with the symmetry breaking as *kd* deviates from zero. This "geometrical" asymmetry leading to a radiation torque has been also observed in the context of elliptical cylinders.[33] Furthermore, verification and validation of the results have been accomplished from the standpoint of energy conservation law applied to scattering, and based on the reciprocity theorem.

References

[1] Awatani J 1955 *Mem. Inst. Scient. Indust. Res., Osaka University* **12** 95
[2] Zhuk A P 1986 *Int. Appl. Mech.* **22** 689
[3] Wu J, Du G, Work S S and Warshaw D M 1990 *J. Acoust. Soc. Am.* **87** 581
[4] Hasegawa T, Saka K, Inoue N and Matsuzawa K 1988 *J. Acoust. Soc. Am.* **83** 1770
[5] Hasegawa T, Hino Y, Annou A, Noda H, Kato M and Inoue N 1993 *J. Acoust. Soc. Am.* **93** 154
[6] Jamali J, Naei M H, Honarvar F and Rajabi M 2011 *J. Mech.* **27** 227
[7] Mitri F G 2006 *New J. Phys.* **8** 138
[8] Mitri F G 2005 *Eur. Phys. J. B* **44** 71
[9] Mitri F G 2005 *J. Sound Vib.* **284** 494
[10] Mitri F G 2005 *Ultrasonics* **43** 271
[11] Haydock D 2005 *J. Phys. A: Math. Gen.* **38** 3279
[12] Wang J T and Dual J 2009 *J. Phys. A: Math. Theor.* **42** 285502
[13] Mitri F G 2015 *Ultrasonics* **62** 244
[14] Mitri F G 2015 *AIP Adv.* **5** 097205
[15] Mitri F G 2016 *Wave Motion* **66** 31
[16] Mitri F G 2017 *Ultrasonics* **73** 236
[17] Mitri F G 2016 *J. Appl. Phys.* **120** 104901
[18] Gao S, Mao Y W, Liu J H and Liu X Z 2018 *Chin. Phys. B* **27** 014302
[19] Roumeliotis J A and Kakogiannos N B 1995 *J. Acoust. Soc. Am.* **97** 2074
[20] Danila E B, Conoir J M and Izbicki J L 1998 *Acta Acust. United Ac.* **84** 38
[21] Hasheminejad S M and Alibakhshi M A 2008 *J. Zhejiang University-Sci. A* **9** 65
[22] Hasheminejad S M and Kazemirad S 2008 *J. Sound Vib.* **318** 506
[23] Hasheminejad S M and Kazemirad S 2008 *Acta Acust. United Ac.* **94** 79
[24] Morse P M and Feshbach H 1953 *Methods of theoretical physics*, Vol 2 (New York: McGraw-Hill Book Co.)
[25] Ivanov E A 1970 *Diffraction of electromagnetic waves on two bodies* ((Minsk: Nauka i Tekhnika Press), NASA Technical Translation F-597)
[26] Mitri F G 2017 *J. Appl. Phys.* **121** 144904
[27] Mitri F G 2017 *J. Phys. Commun.* **1** 055015
[28] Maidanik G 1958 *J. Acoust. Soc. Am.* **30** 620
[29] Wiscombe W J 1980 *Appl. Optics* **19** 1505
[30] Mitri F G 2015 *Ultrasonics* **62** 20
[31] Varatharajulu V 1977 *J. Math. Phys.* **18** 537
[32] Mitri F G 2017 *J. Appl. Phys.* **121** 144901
[33] Mitri F G 2016 *Phys. Fluids* **28** 077104